

First direct detection constraints on eV-scale hidden-photon dark matter with DAMIC at SNOLAB

A. Aguilar-Arevalo,¹ D. Amidei,² X. Bertou,³ M. Butner,^{4,5} G. Canelo,⁴ A. Castañeda Vázquez,¹ B.A. Cervantes Vergara,¹ A.E. Chavarria,⁶ C.R. Chavez,⁷ J.R.T. de Mello Neto,⁸ J.C. D'Olivo,¹ J. Estrada,⁴ G. Fernandez Moroni,^{4,9} R. Gaïor,¹⁰ Y. Guardincerri,⁴ K.P. Hernández Torres,¹ F. Izraelevitch,⁴ A. Kavner,² B. Kilminster,¹¹ I. Lawson,¹² A. Letessier-Selvon,¹⁰ J. Liao,¹¹ A. Matalon,⁶ V.B.B. Mello,⁸ J. Molina,⁷ P. Privitera,⁶ K. Ramanathan,⁶ Y. Sarkis,¹ T. Schwarz,² M. Settimo,¹⁰ M. Sofo Haro,³ R. Thomas,⁶ J. Tiffenberg,⁴ E. Tiouchichine,³ D. Torres Machado,⁸ F. Trillaud,¹ X. You,⁸ and J. Zhou⁶

(DAMIC Collaboration)

¹ *Universidad Nacional Autónoma de México, Mexico City, Mexico*

² *Department of Physics, University of Michigan, Ann Arbor, MI, United States*

³ *Centro Atómico Bariloche - Instituto Balseiro, CNEA/CONICET, Argentina*

⁴ *Fermi National Accelerator Laboratory, Batavia, IL, United States*

⁵ *Northern Illinois University, DeKalb, IL, United States*

⁶ *Kavli Institute for Cosmological Physics and The Enrico Fermi Institute, The University of Chicago, Chicago, IL, United States*

⁷ *Facultad de Ingeniería - Universidad Nacional de Asunción, Paraguay*

⁸ *Universidade Federal do Rio de Janeiro, Instituto de Física, Rio de Janeiro, RJ, Brazil*

⁹ *Universidad Nacional del Sur, Bahía Blanca, Argentina*

¹⁰ *Laboratoire de Physique Nucléaire et de Hautes Energies (LPNHE), Universités Paris 6 et Paris 7, CNRS-IN2P3, Paris, France*

¹¹ *Universität Zürich Physik Institut, Zurich, Switzerland*

¹² *SNOLAB, Lively, ON, Canada*

(Dated: November 10, 2016)

We present direct detection constraints on the absorption of hidden-photon dark matter with particle masses in the range $1.2\text{--}30\text{ eV } c^{-2}$ with the DAMIC experiment at SNOLAB. Under the assumption that the local dark matter is entirely constituted of hidden photons, the sensitivity to the kinetic mixing parameter κ is competitive with constraints from solar emission, reaching a minimum value of 2.2×10^{-14} at $17\text{ eV } c^{-2}$. These results are the most stringent direct detection constraints on hidden-photon dark matter with masses $3\text{--}12\text{ eV } c^{-2}$ and the first demonstration of direct experimental sensitivity to ionization signals $<12\text{ eV}$ from dark matter interactions.

The DAMIC (Dark Matter in CCDs) experiment at SNOLAB [1] employs the bulk silicon of scientific-grade charge-coupled devices (CCDs) as a target for ionization signals produced by interactions of particle dark matter. Because of the characteristics of CCD operation, signals from particle interactions that would individually be indistinguishable from readout noise can be integrated over long exposures to obtain a detectable cumulative signal. Thus, the devices are sensitive to ionization signals as small as a single electron, which can occur from interactions that deposit sufficient energy to overcome the band gap of silicon (1.2 eV).

In this letter, we report on a search for hidden photons (HPs), well-motivated dark matter candidates [2] that, in an analogous manner to the photons from electromagnetism, can be absorbed by electrons and lead to ionization in the bulk silicon. The absorption cross section for HPs [3–5] is determined by the kinetic mixing κ between the field strength tensors of electromagnetism and its “hidden” counterpart. When in-medium dispersion effects are considered, an effective mixing parameter κ_{eff} can be defined such that the absorption cross section for a non-relativistic HP of mass m_V in the medium, $\sigma_V(m_V)$, is related to the photoelectric cross section for

a photon with energy $m_V c^2$, $\sigma_\gamma(m_V c^2)$, by

$$\sigma_V(m_V)v = \kappa_{eff}^2 \sigma_\gamma(m_V c^2)c,$$

where v is the speed of the HP in the laboratory frame and c is the speed of light. The effective kinetic mixing can be expressed as

$$\kappa_{eff}^2 = \frac{\kappa^2 m_V^4}{(m_V^2 - \text{Re}[\Pi(m_V c^2)])^2 + (\text{Im}[\Pi(m_V c^2)])^2},$$

where $\Pi(m_V c^2)$ is the polarization tensor of the medium evaluated at a photon energy equal to the HP rest mass.

Hence, for a detector target located within the dark matter halo the absorption rate of HPs would be

$$\Gamma = \frac{\rho_{DM}}{m_V} \kappa_{eff}^2 \sigma_\gamma(m_V c^2)c, \quad (1)$$

where $\rho_{DM}=0.3\text{ GeV } c^{-2}\text{ cm}^{-3}$ is the local density of dark matter. Of particular relevance is the lack of dependence of Γ on v , the result being insensitive to the details of the HP velocity distribution in the dark matter halo. Thus, unlike searches for weakly-interacting massive particles (WIMPs) by elastic scattering off nuclei, no annual modulation is expected in the potential signal.

The search for HPs was performed with 6.25 d of data acquired in January 2016 with a $4k \times 4k$ -pixel CCD (5.8 g in mass) deployed as part of the R&D program of the DAMIC experiment. This device exhibited the lowest leakage current of four CCDs installed in the DAMIC copper box when cooled to 105 ± 5 K inside a copper vacuum vessel ($\sim 10^{-6}$ mbar). The setup was shielded on all sides by at least 18 cm of lead and 42 cm of polyethylene to stop background radiation from environmental γ -rays and neutrons, respectively. Details of the DAMIC infrastructure at SNOLAB can be found in Refs. [1, 6].

The CCD features a three-phase polysilicon gate structure with a buried p-channel. The pixel size is $15 \times 15 \mu\text{m}^2$ and the bulk of the device is high-resistivity (10–20 k Ω cm) n-type silicon with a substrate thickness of 675 μm . The high resistivity of the silicon allows for a low donor density in the substrate ($\sim 10^{11} \text{ cm}^{-3}$), which leads to fully depleted operation at a substrate bias of 40 V. Ionization charge produced in the bulk is drifted along the direction of the electric field across the substrate. The holes (charge carriers) are collected and held near the p-n junction, less than 1 μm below the gates. Because of thermal motion, the ionized charge diffuses transversely with respect to the electric field direction as it is drifted, with a lateral variance that is proportional to the carrier transit time. The ionized charge is held at the CCD gates until it is read out. During readout, the charge is transferred in the y direction from pixel to pixel along each column by appropriate clocking of the three-phase gates (“parallel clocks”), while higher frequency clocks (“serial clocks”) move the charge of the last row (the “serial register”) in the x direction to the primary CCD output node, where the charge is measured by a correlated double-sampling circuit [7]. DAMIC CCDs have a second output node on the other end of the serial register in which charge is not deposited, offering a measurement of zero charge, i.e., of noise. The inefficiency of charge transfer from pixel to pixel is as low as 10^{-6} [8] and the readout noise in the charge measurement is $\sim 2 e^-$ [1]. The image is reconstructed from the order in which the pixels are read out, and contains a two-dimensional stacked history (projected on the x - y plane) of all ionization produced throughout the exposure. The data used for this analysis was acquired in a 1×100 acquisition mode, meaning that 100 rows were transferred into the serial register before the charge was clocked in the x direction and each column segment was read out individually. Thus, each image pixel is effectively $15 \times 1500 \mu\text{m}^2$ in size. For details in the acquisition modes of DAMIC CCDs see Ref. [1].

Nine exposures of 0.695 d each were acquired with images 4622×60 pixels in size. The device was brought into inversion before every exposure to suppress surface dark current [7]. The CCD data is contained in a 4116×42 -pixel segment of the image, corresponding to the physical size of the device, with the remaining regions constituting the “overscan,” where the CCD was clocked in both x and y directions beyond its active region to obtain mea-

surements of zero charge with the primary output node. Images were also acquired with the secondary CCD output node and with the other three CCDs installed in the DAMIC box. Since the readout of all images is synchronized by the clocking, the noise images by the second output nodes of all CCDs allow for the identification and suppression of correlated electronic noise of the detector’s readout chain.

The output of a CCD readout chain is recorded in Analog-to-Digital converter Units (ADU) proportional to the number of charge carriers placed in the CCD’s output node. The linear constant α relating the pixel value to the number of charge carriers, was calibrated before deployment with x-ray lines of known energy to be $\alpha = 0.0727 e^-/\text{ADU}$. The linearity of the CCD output was confirmed within $\pm 10\%$ for signals as small as $2 e^-$ using optical photons [1].

The image processing started with the subtraction of the pedestal (the constant offset of the pixel values introduced at the time of readout) from every pixel. The pedestal was estimated independently for each row as the mean value of the pixels in the x overscan. To exclude a slight pedestal transient at the beginning of every row, the analysis was limited to the last 2500 columns of the image, for which the pixel values along rows in the y overscan were found to be constant within statistical uncertainty. To remove correlated readout noise, from every pixel we subtracted a linear combination of the pixel values in the corresponding four noise images, with the coefficients determined as to minimize the variance of the pixel noise. Following this procedure, the noise in the images was estimated from the pixel values of the y overscan to be $\sigma_{\text{pix}} = 1.9 e^-$.

We calculated the median and median absolute deviation (MAD) of every pixel over 114 images from a previous higher-temperature data set dedicated to background studies. These quantities were used to construct a mask, which excludes localized dark current spikes due to defects in the silicon lattice [7]. These were identified as pixels that either deviate more than 3 MAD from the median in at least 50% of the images or have a median or MAD that is an outlier when compared to the distributions of these variables for all pixels. This selection removed 0.17% of the pixels.

This analysis was restricted to the lowest energy signals, thus ionization events that could be individually identified with high significance over pixel noise were masked from the image. These events were defined as clusters of contiguous pixels with signal larger than $6 \sigma_{\text{pix}}$, corresponding to > 43 eV of detected energy (on average, 3.8 eV are required to produce a free charge carrier in silicon [9]). Pixels that are less than 4 pixels to the right of the cluster and pixels that are less than 200 pixels to the left of the cluster, i.e., within the 200 subsequent pixel readouts, were also masked. This condition rejected pixels with stray charge due to CCD charge transfer inefficiencies, which may happen when a high energy interaction results in a large number of charge carriers in

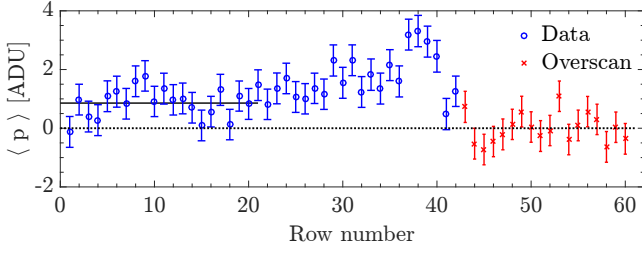


FIG. 1. Mean of the pixel values in each row over the nine images, $\langle p \rangle$, as a function of row number. The first 42 rows contain the CCD data, while the remaining 18 rows constitute the y overscan. The dotted line shows $\langle p \rangle = 0$, while the solid line presents the level of leakage charge that corresponds to $\lambda = 4.0 e^- \text{ mm}^{-2} \text{ d}^{-1}$.

the serial register. Because of the low event rate from radioactive backgrounds ($\sim 1 \text{ g}^{-1} \text{ d}^{-1}$), only 0.95% of the pixels were removed by this procedure.

Figure 1 shows the mean value of pixels in each row over the nine images, $\langle p \rangle$, after the image processing and pixel selection described above. Rows ≥ 43 correspond to the y overscan, for which $\langle p \rangle$ is consistent with zero. The first 42 rows of the image contain the CCD data, for which an offset is clearly visible due to charge collected by the pixels. HP absorption would produce charge uniformly distributed throughout the pixel array. The higher values of collected charge in rows 30–40 indicate the presence of non-uniform sources of leakage current, e.g., optical or near-infrared photons inside the vessel or dark current exacerbated by mechanical stress of the silicon lattice. The same pattern is more clearly observed in the other CCDs with higher leakage current installed in the DAMIC box, with a spatially uniform charge distribution in the bottom-half of the devices, i.e., rows 1–21.

Thus, we consider rows 1–21 to place upper limits on the possible contribution to the collected charge from HP absorption. This selection corresponds to $N = 4.68 \times 10^5$ unmasked pixels over the nine images, equivalent to an exposure of 11.5 g d . The distribution of pixel values (Figure 2) can be described as a function of the pixel value in ADU, p , by

$$f(p) = N \sum_{n=0}^{\infty} F(n|\lambda, \Gamma, m_V) \text{Gaus}(\alpha p | n - \mu_0, \sigma_{\text{pix}}),$$

where the sum is over the number of carriers collected by a pixel, n , each multiplied by a Gaussian function that describes the pixel white noise with mean n and standard deviation σ_{pix} , and relative frequencies, F , that depend on the leakage current per unit area, λ , and the HP absorption rate, Γ . An offset, μ_0 , that could remain because of the statistical uncertainty in the subtraction of the pedestal was included in the function.

In the absence of charge from HP absorption, i.e., for the case of the “null” hypothesis, F reduces to the contribution from leakage current:

$$F(n|\lambda, 0, m_V) = \text{Poisson}(n|\mathcal{E}\lambda), \quad (2)$$

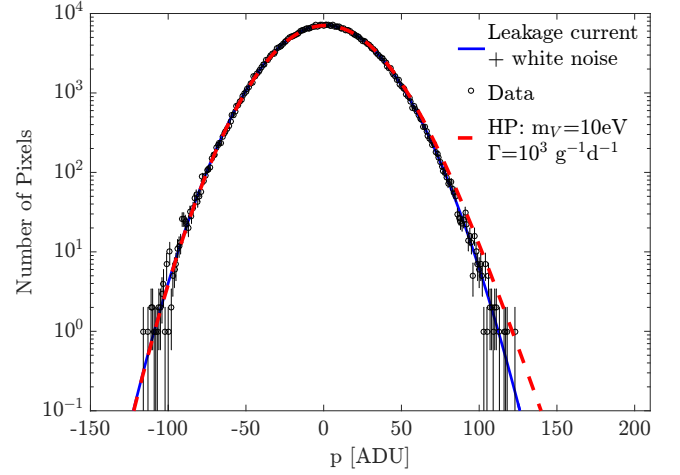


FIG. 2. Distribution of the pixel values, p , considered for this analysis (markers). The solid line shows the best-fit result with the null hypothesis, i.e., only pixel white noise and a constant leakage current source across the device. The p-value is 0.78. The dashed line shows the result after including a fixed contribution from HPs with mass $m_V = 10 \text{ eV}$ and an absorption rate of $\Gamma = 10^3 \text{ g}^{-1} \text{ d}^{-1}$.

modeled as a Poisson distribution under the assumption of uncorrelated production of charge carriers uniformly distributed across the selected region of the CCD. The mean leakage charge collected by a pixel is proportional to the image single pixel exposure of $\mathcal{E} = 0.0156 \text{ mm}^2 \text{ d}$.

To obtain the contribution to F from the charge generated by HP absorption we rely on Monte Carlo simulations. For a given HP mass m_V , we simulated a number of interactions drawn from a Poisson distribution with mean $\Gamma N \mathcal{E} \rho$, where ρ is the CCD density of 1.57 mg mm^{-2} . We randomly selected the spatial position of the HP absorption uniformly in depth and within the selected region of the CCD. For each simulated HP absorption, we generated the number of charge carriers as for the photoelectric absorption of a photon with energy $m_V c^2$, using the probability distributions from Ref. [10]. We then distributed the carriers on the pixel array according to the charge diffusion model for the CCD, described and validated in Ref. [1]. A histogram was made of the contents of all pixels in the simulated pixel array, and the simulation was repeated 100 times to obtain a numerical distribution of $F(n|0, \Gamma, m_V)$. This function was then convolved with Eq. 2 to obtain $F(n|\lambda, \Gamma, m_V)$.

We first performed a likelihood fit to the data with the null hypothesis, with σ_{pix} , λ and μ_0 as free parameters. Two penalty terms were added in the log-likelihood definition to include in the fit the prior knowledge of the values of σ_{pix} and μ_0 . The value of σ_{pix} was constrained to the result from a fit to the pixels in the y overscan, while μ_0 was constrained within the statistical uncertainty in the pedestal subtraction. The best-fit result has a p-value of 0.78, with best-fit values of $\sigma_{\text{pix}} = 1.889 \pm 0.002 e^-$, $\lambda = 4.0 \pm 0.4 e^- \text{ mm}^{-2} \text{ d}^{-1}$ and $\mu_0 = 0.010 \pm 0.005 e^-$.

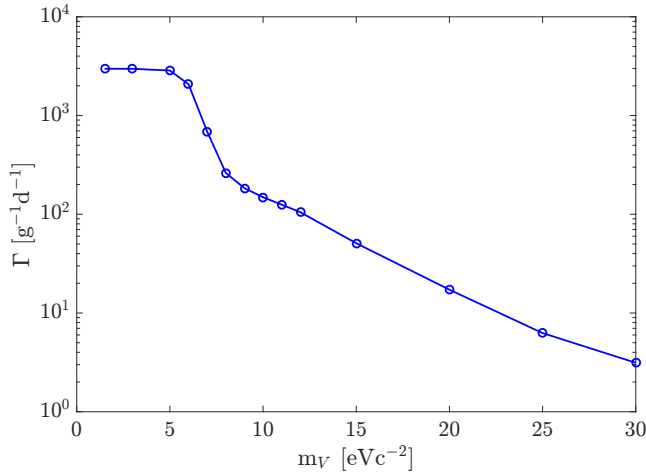


FIG. 3. Upper limits (90% C.L.) on the HP absorption rate, Γ , as a function of HP mass, m_V , obtained from the likelihood fit described in the text.

To explore the HP signal, we performed a scan for values of m_V and Γ . For each value of m_V , we increased the value of Γ in discrete steps starting from zero. At every step, the likelihood fit was performed where the parameters m_V and Γ were fixed and σ_{pix} , λ and μ_0 were free. The minimum log-likelihood was registered and a likelihood profile was constructed for every m_V as a function of Γ . There was no statistical significance of a HP signal for any m_V . The 90% C.L. upper limit on Γ was thus obtained from the likelihood profile using a likelihood-ratio test. Figure 3 presents the results as a function of m_V from 1.2 to 30 $\text{eV } c^{-2}$.

Below $5 \text{ eV } c^{-2}$, HP absorptions produce only one charge carrier, leading to a current source that would be indistinguishable from leakage current, and an upper limit on the absorption rate at the same level as the leakage current. At higher m_V , the multiplicity in the number of carriers produced per absorption increases, leading to pixels that collect significantly more carriers than would be expected from leakage current. This leads to a longer tail on the right side of the pixel distribution, and consequently to a stronger upper limit on Γ . As an example, the dashed line in Figure 2 shows the best-fit result with fixed parameters $m_V = 10 \text{ eV}$ and $\Gamma = 10^3 \text{ g}^{-1} \text{ d}^{-1}$.

The absorption rate, Γ , is related to the HP kinetic mixing, κ , through κ_{eff} according to Eq. 1. We use this relation to translate the upper limit on Γ for a given m_V to the corresponding upper limit on κ . Following Ref. [4], we compute the polarization tensor using the complex index of refraction in silicon, estimated at the detector operating temperature of 105 K by extrapolating the values given in Ref. [11] using the empirical parameterization from Ref. [12]. The results are shown in Figure 4.

Several sources of systematic uncertainty were investigated. The largest effect arises from the uncertainty in the linearity of the CCD output signal, which we estimated by varying α by $\pm 10\%$, resulting in changes in the

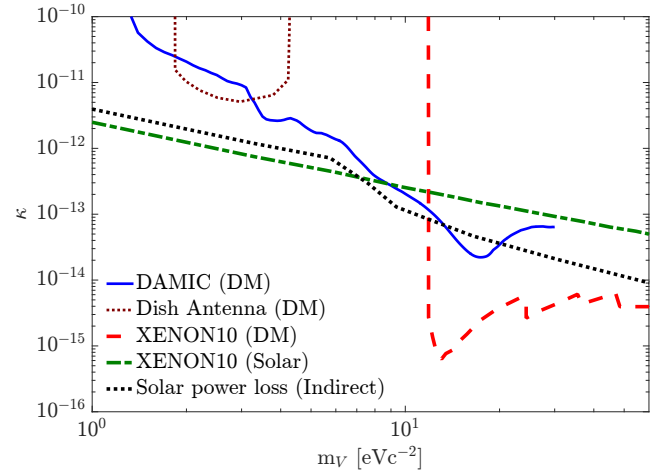


FIG. 4. Exclusion plot (90% C.L.) for the HP kinetic mixing, κ , as a function of HP mass, m_V , from the dark matter search presented in this letter (solid line). The exclusion limits from other direct searches for HP dark matter in the galactic halo with a dish antenna (thin-dotted line) [13] and with the XENON10 experiment (dashed line) [5] are shown for comparison. A limit from a direct search with the XENON10 experiment for HPs radiated by the Sun (dot-dashed line) [5] and an indirect constraint from the upper limit of the power lost by the Sun into invisible radiation (thick-dotted line) [14] are also presented.

upper limit of Γ ranging from 10% for $m_V < 5 \text{ eV } c^{-2}$ up to a factor of 2 for $m_V = 30 \text{ eV } c^{-2}$. We repeated the analysis for different selected regions of the CCD. Restricting the analysis to the last 2200 columns or considering rows 1–18 leads to $< 20\%$ changes in the upper limits of Γ . We confirmed the absence of pixels with values from 6 to $8 \sigma_{\text{pix}}$, thus the result is insensitive to the upper bound on the pixel values. Finally, varying the temperature by $\pm 10 \text{ K}$ had a $< 5\%$ impact on the upper limits of κ .

The exclusion limits presented in this letter are the most stringent direct detection constraints on HP dark matter with masses 3–12 $\text{eV } c^{-2}$. The sensitivity of the experiment is approaching that of searches for HP emission by the Sun, offering a complementary technique for their detection. Continued identification and mitigation of dark current and light sources in DAMIC will improve the sensitivity, making CCDs promising direct probes for HP dark matter with eV-scale masses. In addition, this work characterizes the noise sources of DAMIC and demonstrates the sensitivity of the experiment to interactions that produce as little as a single electron, corresponding to ionization signals as small as 1.2 eV.

We thank Tongyan Lin for motivating discussions on HP dark matter. We are grateful to SNOLAB and its staff for support through underground space, logistical and technical services. SNOLAB operations are supported by the Canada Foundation for Innovation and the Province of Ontario Ministry of Research and Innovation, with underground access provided by Vale at the Creighton mine site. We acknowledge the financial

support from the following agencies and organizations: Kavli Institute for Cosmological Physics at the University of Chicago through Grants No. NSF PHY-1125897 and No. PHY-1506208 and an endowment from the Kavli Foundation; Fermi National Accelerator Laboratory (Contract No. DE-AC02-07CH11359); Institut Lagrange de Paris Laboratoire d'Excellence (under Reference No. ANR-10-LABX-63) supported by French state funds managed by the Agence Nationale de la Recherche within the Investissements d'Avenir program under Reference No. ANR-11-IDEX-0004-02; Swiss National Sci-

ence Foundation through Grant No. 200021_153654 and via the Swiss Canton of Zurich; Mexico's Consejo Nacional de Ciencia y Tecnología (Grant No. 240666) and Dirección General de Asuntos del Personal Académico - Universidad Nacional Autónoma de México (Programa de Apoyo a Proyectos de Investigación e Innovación Tecnológica Grants No. IB100413 and No. IN112213); Brazil's Coordenação de Aperfeiçoamento de Pessoal de Nível Superior, Conselho Nacional de Desenvolvimento Científico e Tecnológico, and Fundação de Amparo à Pesquisa do Estado de Rio de Janeiro.

-
- [1] A. Aguilar-Arevalo *et al.* (DAMIC), *Phys. Rev.* **D94**, 082006 (2016), [arXiv:1607.07410 \[astro-ph.CO\]](#).
 - [2] M. Pospelov, A. Ritz, and M. B. Voloshin, *Phys. Rev.* **D78**, 115012 (2008), [arXiv:0807.3279 \[hep-ph\]](#); J. Redondo and M. Postma, *JCAP* **0902**, 005 (2009), [arXiv:0811.0326 \[hep-ph\]](#); A. E. Nelson and J. Scholtz, *Phys. Rev.* **D84**, 103501 (2011), [arXiv:1105.2812 \[hep-ph\]](#); P. Arias *et al.*, *JCAP* **1206**, 013 (2012), [arXiv:1201.5902 \[hep-ph\]](#).
 - [3] H. An, M. Pospelov, J. Pradler, and A. Ritz, *Phys. Lett.* **B747**, 331 (2015), [arXiv:1412.8378 \[hep-ph\]](#).
 - [4] Y. Hochberg, T. Lin, and K. M. Zurek, (2016), [arXiv:1608.01994 \[hep-ph\]](#).
 - [5] I. M. Bloch, R. Essig, K. Tobioka, T. Volansky, and T.-T. Yu, (2016), [arXiv:1608.02123 \[hep-ph\]](#).
 - [6] A. Aguilar-Arevalo *et al.* (DAMIC), *JINST* **10**, P08014 (2015), [arXiv:1506.02562 \[astro-ph.IM\]](#).
 - [7] J. Janesick, *Scientific Charge-Coupled Devices*, Press Monographs (The International Society for Optical Engineering, Bellingham, WA, 2001).
 - [8] S. Holland *et al.*, *IEEE Trans. Electron Devices* **50**, 225 (2003).
 - [9] R. D. Ryan, *IEEE Trans. Nucl. Sci.* **20**, 473 (1973).
 - [10] R. C. Alig, S. Bloom, and C. W. Struck, *Phys. Rev.* **B22**, 5565 (1980); F. Scholze, H. Rabus, and G. Ulm, *J. Appl. Phys.* **84**, 2926 (1998).
 - [11] D. F. Edwards, in *Handbook of Optical Constants of Solids*, edited by E. D. Palik (Academic Press, Burlington, 1997) pp. 547 – 569.
 - [12] K. Rajkanan, R. Singh, and J. Shewchun, *Solid-State Electron.* **22**, 793 (1979).
 - [13] J. Suzuki, T. Horie, Y. Inoue, and M. Minowa, *JCAP* **1509**, 042 (2015), [arXiv:1504.00118 \[hep-ex\]](#).
 - [14] J. Redondo and G. Raffelt, *JCAP* **1308**, 034 (2013), [arXiv:1305.2920 \[hep-ph\]](#).